




Cite this: *Chem. Commun.*, 2024, 60, 6957

Received 10th May 2024,  
Accepted 7th June 2024

DOI: 10.1039/d4cc02281e

rsc.li/chemcomm

# Carbazole-embedded *p*-benzoporphyrinoid: synthesis, structure and a reversible chemodosimeter for mercury(II) ions†

Athira Naniyil, Naveen Korothe Valappil, Alex P. Andrews and Sabapathi Gokulnath \*

**The first carbazole-embedded *p*-benzoporphyrinoid is synthesized by a [3+1] acid-catalyzed condensation between appropriate coupling partners. The macrocycle **1** exhibited orange emission and showed a large Stokes shift of 5831 cm<sup>-1</sup>. Intriguingly, it shows a selective affinity towards Hg<sup>2+</sup> ions over other metal-ions in a reversible manner. Job's plot confirmed the 1:1 stoichiometry with unambiguous confirmation of both **1** and **1**-Hg by single crystal X-ray analysis.**

Porphyrins, a unique class of intensely colored pigments, were studied by scientists as tunable and excellent hosts for diverse metal ions. Due to their large  $\pi$ -conjugated system, they often respond to small changes that can be detected *via* UV-vis absorption, fluorescence and other spectroscopic techniques.<sup>1</sup> The scope of research on porphyrins has broadened with the emergence of core-modified porphyrins.<sup>2</sup> Porphyrins with fused aromatic units have gained popularity owing to their fascinating optical and electrical characteristics with a wide range of applications.<sup>3</sup> In this context, using carbazole as a building block to synthesize modified porphyrinoids is an attractive approach due to its highly emissive properties ( $\phi_F = 0.367$ ), electron-conducting capabilities and chemical stability during organic transformations.<sup>4</sup>

The first carbazole-incorporated porphyrinoid was reported in 2004 by Sessler and co-workers.<sup>5</sup> Subsequently, various researchers have employed different synthetic routes to achieve carbazole-based porphyrinoids, aiming to fine-tune the structure and properties.<sup>6</sup> Incorporating phenylene rings into the porphyrin core offers a distinct change in the aromaticity, flexible structures, varied coordination and optical properties.<sup>2</sup> Benzoporphyrinoids are versatile organometallic ligands that offer

metal–arene interactions inside the macrocyclic core.<sup>7</sup> Coordination chemistry of such systems led to new organometallic complexes *via* activation of arene C–H bonds.<sup>8</sup> It has been shown that *p*-benzoporphyrins form divalent metal complexes with Cd, Ni and Zn-salts with weak  $\eta^2$ -metal–arene interactions.<sup>9</sup>

Mercury, a potent neurotoxin, poses significant environmental and health risks due to its widespread presence in natural ecosystems and industrial processes.<sup>10</sup> The urgent need for accurate and sensitive detection methods has driven extensive research into developing advanced sensor technologies.<sup>11</sup> The past few decades have witnessed increasing interest in the development of optical sensors for Hg<sup>2+</sup> with different chemical transducers, simple operation, rapid response and economic value.<sup>10,12</sup> Among these, porphyrin-based mercury sensors have emerged as a promising class of molecules to detect and quantify mercury ions with exceptional precision. In 2006, Wong and coworkers reported a “turn-OFF” chemo-dosimeter (**A**) that is highly selective towards Hg<sup>2+</sup> ions with an intense NIR fluorescence (Fig. 1).<sup>13</sup> In 2013, Lodeiro and coworkers reported the sensing ability of benzoporphyrins (**B**) towards Zn<sup>2+</sup>, Hg<sup>2+</sup>, Cu<sup>2+</sup>, and Cd<sup>2+</sup> ions.<sup>14</sup> Subsequently, Chauhan and coworkers have shown selective binding of Hg<sup>2+</sup> using a series of core-modified calix[4]pyrroles (**C**).<sup>15</sup> Later in 2014, Lee and coworkers have demonstrated the necessity of soft S-donors for high affinity towards Hg<sup>2+</sup> using a calix[4]pyrrole-based receptor (**D**).<sup>16</sup> In 2015, Ravikanth and coworkers reported a stable calixazasmaragdyrin (**E**) which selectively binds Hg<sup>2+</sup> ions.<sup>17</sup> However, searching for new fluorophores with high selectivity towards toxic metal-ion sensing (Hg<sup>2+</sup>, Cd<sup>2+</sup>) with excellent photostability, large Stokes shifts and high quantum yields is still an ongoing challenge towards sensor applications.

Recently our group has reported various carbazole-based macrocycles exhibiting dual-emissive and excitonically coupled chromophores.<sup>18,19</sup> Subsequently, we have also demonstrated a carbazole-embedded furan-containing macrocycle that showed distinct and reversible mercury binding (**F**).<sup>4</sup> On the contrary, an inverted pyrrole-containing carbazole-embedded macrocycle

School of Chemistry, Indian Institute of Science Education and Research Thiruvananthapuram-695551, Maruthamala P.O., Vithura, Kerala, India.  
E-mail: gokul@iisertrm.ac.in

† Electronic supplementary information (ESI) available: Synthesis, characterization methods and results. CCDC 2350793 (**1**) and 2350794 (**1**-Hg). For ESI and crystallographic data in CIF or other electronic format see DOI: <https://doi.org/10.1039/d4cc02281e>



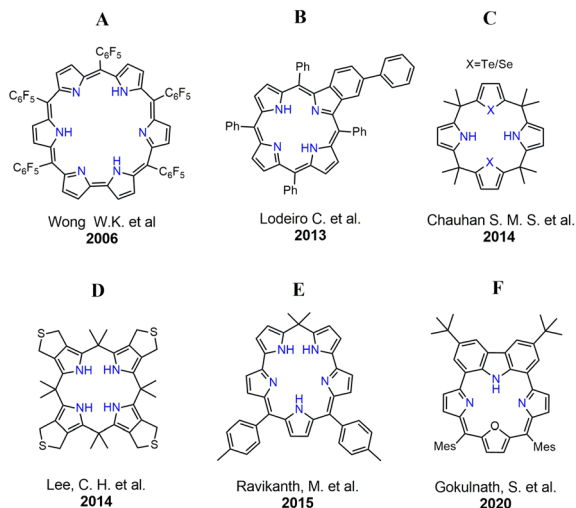
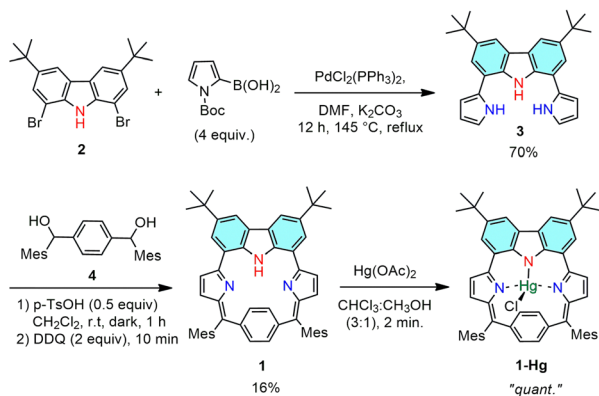


Fig. 1 Previously reported Hg(II) sensors based on porphyrinoids.

selectively binds toxic  $F^-$  and  $CN^-$  ions.<sup>20</sup> In this work, we have modified our design strategy by incorporating a 1,4-phenylene unit embedded with a carbazole subunit for the first time. Intriguingly, such a modification resulted in a large Stokes shift and serves as a reversible turn-OFF  $Hg^{2+}$  chemo-dosimeter in the visible to near-infrared (NIR) range.<sup>21</sup> However, relatively small Stokes shifts of the fluorophores result in severe overlap between the excitation and emission spectra leading to poor signal-to-noise ratios. Thus, in general, a larger Stokes shift is advantageous to achieve sensitive detection.<sup>22</sup>

The synthesis of **1** and **1-Hg** is presented in Scheme 1. The starting material **2** was synthesized by following the literature procedure.<sup>23</sup> Then, the key precursor **3** was prepared by slightly modifying our previously reported procedure *via* adopting a Suzuki–Miyaura coupling reaction at 145 °C, using DMF as a solvent and avoiding the deprotection step.<sup>4</sup> Next, an acid-catalyzed condensation between equimolar amounts of **3** and **1**, 4-phenylenebis(mesityl methanol) **4** was performed using a catalytic amount of *p*-toluenesulfonic acid (*p*-TsOH) in dichloromethane under an argon atmosphere. After 1 hour, a solution of 2,3-dichloro-5,6-dicyano-1,4-benzoquinone (DDQ) in dichloromethane was



Scheme 1 Synthesis of macrocycle **1** and **1-Hg**.

added and the reaction mixture was further allowed to stir for 10 min in open air, which afforded the carbazole-embedded *p*-benzoporphyrinoid **1** as a stable solid in 16% yield. Furthermore, sequential basic alumina and silica gel column chromatographic separations were performed to purify the macrocycle from the polymeric materials formed during the condensation and oxidation processes. The exact composition of the isolated macrocycle **1** was confirmed using high-resolution mass spectral analysis (HRMS-APCI) with  $m/z$ :  $[M + H]^+$ ; calcd for:  $C_{54}H_{53}N_3$ ; 744.4318; found 744.4286 (Fig. S3-1, ESI†).

The UV-vis absorption spectrum of **1** recorded in  $CH_2Cl_2$  displayed three well-defined bands at 290, 375 and 465 nm, respectively (Fig. 2). Upon protonation using dilute  $CF_3COOH$  (TFA) in  $CH_2Cl_2$ , a bathochromic shift of all the bands was observed. Specifically, three bands appeared at 301, 458 and 562 nm, where the band at 301 nm showed a decreased intensity and the two bands at 458 and 562 nm exhibited increased intensities. The fluorescence spectrum of **1** was recorded in  $CH_2Cl_2$  (Fig. 2). Upon photoexcitation ( $\lambda_{ex} = 465$  nm), **1** displayed an orange emission with a band centered at 638 nm. Intriguingly, a large Stokes shift ( $\Delta\tilde{\nu}_{max}$ ) of  $\sim 5831$   $cm^{-1}$  with a very small spectral overlap was observed. Fluorescent probes with large Stokes shifts can effectively avoid self-quenching and overcome interference by the excitation light.<sup>24</sup> The relative fluorescence quantum yield of **1** was determined using a previously reported compound as a reference and the  $\phi_F$  for **1** was found to be 1.25%.<sup>4</sup> Such a low  $\phi_F$  value might be due to active intramolecular rotations of the phenylene subunit and tertiary butyl groups on the carbazole moiety, which serves as a relaxation channel for the excited state to decay.

The  $^1H$  NMR spectrum of **1** in  $CDCl_3$  displayed simple features due to its  $C_2$  symmetric nature (Fig. S4-1, ESI†). A broad signal at 10.06 ppm was ascribed to the NH proton of the carbazole ring. The *p*-phenylene protons resonated as a singlet at 7.31 ppm integrating into four protons presumably due to

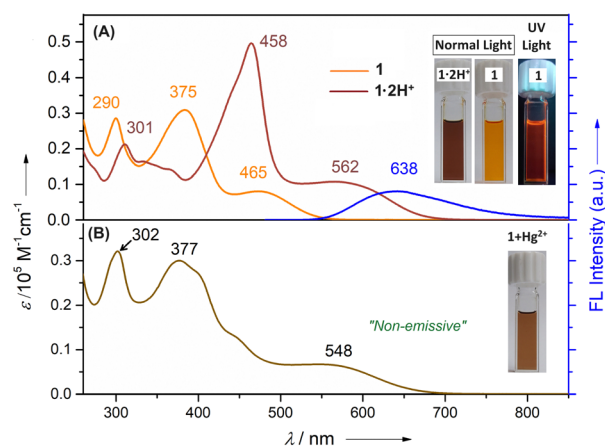


Fig. 2 UV-vis absorption spectra of (A) **1** and **1·2H<sup>+</sup>** along with the fluorescence spectrum of **1** ( $\lambda_{ex} = 465$  nm) in  $CH_2Cl_2$ ; (B) UV-vis absorption spectrum of **1-Hg** in  $CH_2Cl_2$ . Inset: Respective solution colors are shown under normal and UV light.



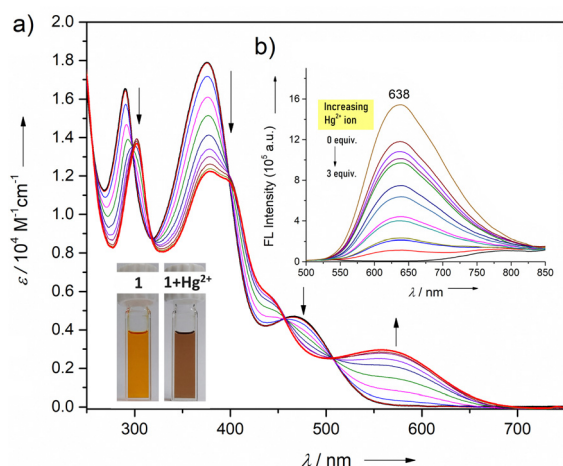


Fig. 3 (a) UV-vis absorption and (b) fluorescence (inset) spectral changes of **1** upon adding methanolic  $\text{Hg}(\text{OAc})_2$  (1 mM of **1**;  $\lambda_{\text{ex}} = 465 \text{ nm}$ ) in  $\text{CHCl}_3$ .

the ring flipping or 'see-saw' motion.<sup>25</sup> The signal for *meta* protons of the *meso*-mesityl rings was observed as a singlet at 7.03 ppm, whereas the peripheral carbazole CH's were observed as two singlets at 8.24 and 8.41 ppm, respectively.

Next, we examined the affinity of **1** with a series of acetate salts of transition-metal ions ( $\text{Mn}^{2+}$ ,  $\text{Fe}^{3+}$ ,  $\text{Co}^{2+}$ ,  $\text{Ni}^{2+}$ ,  $\text{Cu}^{2+}$ ,  $\text{Cd}^{2+}$ ,  $\text{Zn}^{2+}$ ,  $\text{Pd}^{2+}$ ,  $\text{Ag}^+$ , and  $\text{Hg}^{2+}$ ) and some group 1 ( $\text{Li}^+$ ,  $\text{Na}^+$ , and  $\text{Cs}^+$ ) and group 2 ( $\text{Mg}^{2+}$ ,  $\text{Sr}^{2+}$ , and  $\text{Ba}^{2+}$ ) metal ions in alcoholic solution (Fig. S5-5, ESI†). Initial binding using UV-vis absorption studies revealed that only  $\text{Hg}^{2+}$  caused significant spectral changes with a marked increase in the band's intensity at 548 nm. Such binding can be distinguishable by the naked eye with instant color change from orange to brown in  $\text{CH}_2\text{Cl}_2$  and alcoholic solutions. Furthermore, a significant decrease in the fluorescence intensity centered at 638 nm upon the addition of  $\text{Hg}^{2+}$  was observed (Fig. 3). Such a fluorescence quenching most likely results from the cation interactions between the heavy atom and the electron-rich phenylene ring, thereby relaxing *via* a non-radiative pathway.<sup>13</sup> Notably, the addition of other metal ions to **1** did not alter the absorption features significantly (Fig. S5-5, ESI†). Further, Job's plot analysis confirmed the 1:1 stoichiometry of the host-guest complex (Fig. S5-7, ESI†). Additionally,  $\text{Hg}^{2+}$  could be detected down to a concentration of  $10^{-6} \text{ M}$  which is desirable for detecting toxic ions in trace quantities. A linear Stern-Volmer (SV) relationship was obtained from the titration profile and the SV binding constant is calculated to be  $K_{\text{SV}} = 6 \times 10^4 \text{ M}^{-1}$  (Fig. S5-8, ESI†).

The ability of macrocycle **1** to act as a ligand was investigated by the insertion of  $\text{Hg}^{2+}$ -ions inside the macrocyclic core. The Hg-bound complex **1-Hg** was obtained by treating **1** with mercury acetate in  $\text{CHCl}_3/\text{CH}_3\text{OH}$  (3:1) at room temperature. Due to its instability on the silica-gel column, it was directly re-crystallized using hot chloroform. The exact composition of **1-Hg** was confirmed using high-resolution mass spectral analysis (HRMS-APCI) with  $m/z$ :  $[\text{M} + \text{H}]^+$ ; calcd for:  $\text{C}_{54}\text{H}_{52}\text{ClHgN}_3$ ; 980.3634; found 980.3634 (Fig. S3-2, ESI†). The 'see-saw' motion of the phenylene ring observed for the free base *p*-benzporphyrin (**1**)

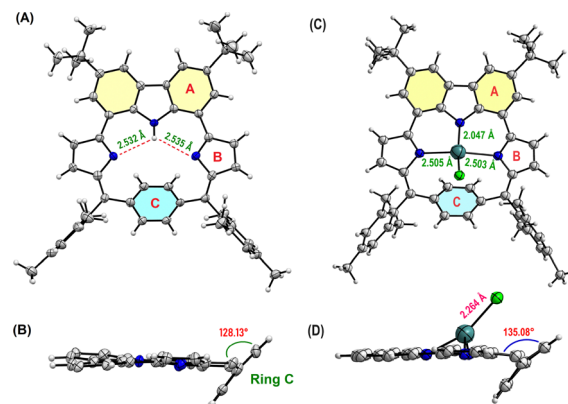


Fig. 4 Crystal structure of **1**: (A) top view and (B) side view; and **1-Hg**: (C) top view and (D) side view. *meso*-Aryl and *tert*-butyl groups have been removed for clarity.

is hindered by the  $\text{Hg}^{2+}$  complexation. As a consequence, the  $^1\text{H}$  NMR spectrum of diamagnetic complex **1-Hg** featured two well-resolved phenylene signals at 7.30 and 7.05 ppm, due to the outer and inner protons, respectively, along with the disappearance of the carbazole-NH signal (Fig. S4-5, ESI†). All the protons were further accounted using  $^1\text{H}$ - $^1\text{H}$  COSY and  $^1\text{H}$ - $^1\text{H}$  ROESY analysis (Fig. S4-6 and S4-7, ESI†). The signals for outer  $\beta$ -pyrrolic (ring B) protons are assigned based on the  $^1\text{H}$ - $^1\text{H}$  COSY correlation exhibited between 7.89 and 7.29 ppm, respectively. The  $^1\text{H}$ - $^1\text{H}$  ROESY spectrum further guided us to distinguish the outer and inner phenylene protons, where only the outer protons showed a correlation with the *o*- $\text{CH}_3$  protons of the mesityl ring.

X-ray quality single crystals of **1** were grown by slow vapor diffusion of hexane into a solution of **1** in chloroform at room temperature (Fig. 4). X-ray diffraction analysis provided unambiguous confirmation revealing that the *p*-phenylene moiety is significantly tilted (*ca.*  $128.13^\circ$ ) from the mean plane. The C-C bond lengths within the phenylene subunit deviate slightly from the ideal benzenoid form, indicating weak conjugation with the rest of the subunits. A closer look into the 2D crystal packing of **1** revealed the presence of two strong intramolecular N-H...N bonding interactions (2.532 Å and 2.534 Å). Furthermore, the solid-state packing array revealed two intermolecular hydrogen bonding interactions (C-H...N; 2.701 Å). Such interactions are observed between the pyrrolic nitrogen of one macrocycle with the methyl hydrogen of the adjacent macrocycle forming dimers in a slip-stacked manner (Fig. S6-3, ESI†). Next, good quality crystals of **1-Hg** were also obtained from the slow vapor diffusion of methanol into a solution of **1-Hg** in chloroform. A boat-like puckering of the *p*-phenylene ring is observed due to the macrocyclic ring strain.<sup>9</sup> Upon Hg-complexation, the steric congestion due to the coordinated Hg-Cl makes the *p*-phenylene subunit more tilted (*ca.*  $135.08^\circ$ ) as compared to **1** (Fig. 4D) (Fig. S6-2, ESI†).

DFT calculations were done at the B3LYP/6-311G(d) level. The calculated HOMO-LUMO gap for **1-Hg** (2.15 eV) is relatively small as compared to **1** (2.76 eV) (Fig. 5). This result is in close agreement with the UV-vis absorption features (Fig. 2). The

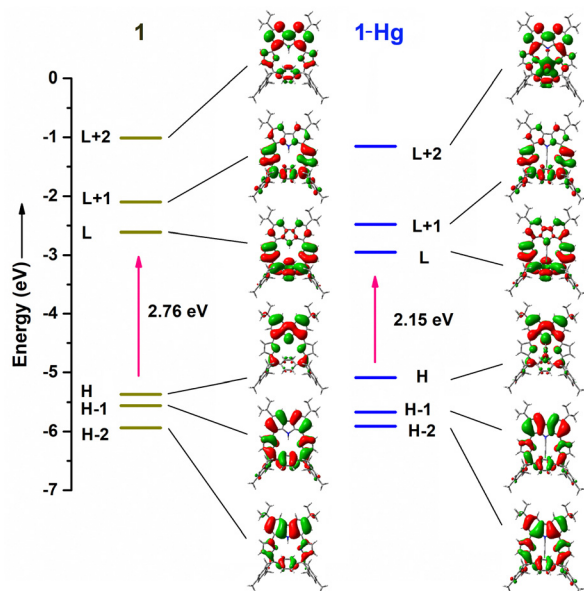


Fig. 5 Energy level diagrams of **1** and **1-Hg** with selected MOs.

Kohn–Sham orbitals of **1** reveal that the electronic coefficients in the HOMO are primarily localized on the carbazole ring, whereas they are more pronounced in the LUMO over the pyrrolinone and *p*-phenylene subunits. The NICS(0) value at the centre of macrocycle **1** was found to be  $-1.35$  ppm, indicating its nonaromatic nature (Fig. S7-1, ESI<sup>†</sup>). Furthermore, the most probable molecular geometry and the corresponding oscillator strength were obtained (Fig. S7-2–S7-4, ESI<sup>†</sup>). The Q-like bands of the macrocycle are related to the transitions from the HOMO or HOMO–1 to LUMO, whereas the transition from HOMO or HOMO–1 to LUMO+1 contributes to the absorption bands at lower wavelengths. Tables S7-1–S7-3 (ESI<sup>†</sup>) represent the impact of the molecular orbitals on the “spectroscopic” transitions of **1**, **1-Hg** and **1-2H<sup>+</sup>**, respectively. The anisotropy of the induced current density (AICD) plot of **1** illustrates the magnetic vectors moving clockwise around the macrocyclic periphery. However, global aromaticity cannot be realized due to the opposite movement of magnetic vectors of the phenylene and carbazole subunits, which prevents global conjugation (Fig. S7-1, ESI<sup>†</sup>).

In summary, we have synthesized a stable carbazole-embedded *p*-benzporphyrinoid **1**, which was structurally characterized. **1** exhibits a large Stokes shift ( $\Delta\tilde{\nu}_{\text{max}} \sim 5831 \text{ cm}^{-1}$ ) which is advantageous over other macrocyclic sensors for the sensitive detection of ions in a selective optical window. Thus, **1** is deemed to be a highly sensitive fluorescent chemo-dosimeter for the selective detection of  $\text{Hg}^{2+}$  ion in a reversible manner. The instant and distinguishable color change through the naked eye makes this probe promising for sensor applications. The presence of inner-CHs through the *p*-phenylene ring can be triggered for metal–carbon bond formation leading to organo-metallic complexes.<sup>24,25</sup> Efforts are underway in our laboratory

toward new metal-sandwich complexes by taking advantage of the phenylene subunits with  $\eta^2$  fashion.

This work was supported by IISER Thiruvananthapuram and SERB Core Research Grant no. CRG/2019/006303. A. N. thanks CSIR for her fellowship.

## Data availability

The experimental and theoretical data supporting this article have been included as part of the ESI<sup>†</sup>.

## Conflicts of interest

There are no conflicts to declare.

## Notes and references

- Z. Qi, Y. Cheng and Z. Xu, *Int. J. Mol. Sci.*, 2020, **21**, 5839–5866.
- P. J. Chmielewski and L. Latos-Grazyński, *Coord. Chem. Rev.*, 2005, **249**, 2510–2533.
- L. Jiang, J. T. Engle, L. Sirk, C. S. Hartley, C. J. Ziegler and H. Wang, *Org. Lett.*, 2011, **13**, 3020–3023.
- A. Kalaiselvan, I. S. Vamsi Krishna, A. P. Nambiar, A. Edwin, V. S. Reddy and S. Gokulnath, *Org. Lett.*, 2020, **22**, 4494–4499.
- P. Piątek, V. M. Lynch and J. L. Sessler, *J. Am. Chem. Soc.*, 2004, **126**, 16073–16076.
- C. Maeda, T. Yoneda, N. Aratani, M. C. Yoon, J. M. Lim, D. Kim, N. Yoshioka and A. Osuka, *Angew. Chem., Int. Ed.*, 2011, **50**, 5691–5694.
- B. Szyszko, L. Latos-Grazyński and L. Sztrenberg, *Angew. Chem., Int. Ed.*, 2011, **50**, 6587–6591.
- M. Ste, *Inorg. Chem.*, 2004, **43**, 6654–6662.
- M. Ste, *J. Am. Chem. Soc.*, 2004, **126**, 4566–4580.
- C. T. Driscoll, R. P. Mason, H. M. Chan, D. J. Jacob and N. Pirrone, *Environ. Sci. Technol.*, 2013, **47**, 4967–4983.
- Q. Li and Y. Zhou, *RSC Adv.*, 2023, **13**, 19429–19446.
- R. Paolesse, S. Nardis, D. Monti, M. Stefanelli and C. Di Natale, *Chem. Rev.*, 2017, **117**, 2517–2583.
- X. J. Zhu, S. T. Fu, W. K. Wong, J. P. Guo and W. Y. Wong, *Angew. Chem., Int. Ed.*, 2006, **45**, 3150–3154.
- N. M. M. Moura, C. Nuñez, S. M. Santos, M. A. F. Faustino, J. A. S. Cavaleiro, M. G. P. M. S. Neves, J. L. Capelo and C. Lodeiro, *ChemPlusChem*, 2013, **78**, 1230–1243.
- S. Ahmad, K. K. Yadav, S. J. Singh and S. M. S. Chauhan, *RSC Adv.*, 2014, **4**, 3171–3180.
- I. Saha, K. H. Park, M. Han, S. K. Kim, V. M. Lynch, J. L. Sessler and C. H. Lee, *Org. Lett.*, 2014, **16**, 5414–5417.
- T. Chatterjee, S. Areti and M. Ravikanth, *Inorg. Chem.*, 2015, **54**, 2885–2892.
- A. Kalaiselvan, A. Spergen, I. S. V. Krishna, V. S. Reddy and S. Gokulnath, *Chem. Commun.*, 2021, **57**, 4420–4423.
- A. Kalaiselvan, S. Dhamija, C. Aswathi, A. K. De and S. Gokulnath, *Chem. Commun.*, 2021, **57**, 11485–11488.
- A. Kalaiselvan, A. Naniyil, R. M. Ipe, S. V. Krishna Isukapalli, S. R. Vennapusa, A. P. Andrews and S. Gokulnath, *J. Org. Chem.*, 2023, **88**, 14377–14387.
- H. Shuai, C. Xiang, L. Qian, F. Bin, L. Xiaohui, D. Jipeng, Z. Chang, L. Jiahui and Z. Wenbin, *Dyes Pigm.*, 2021, **187**, 109125.
- J. Zhang, M. Moemeni, C. Yang, F. Liang, W. T. Peng, B. G. Levine, R. R. Lunt and B. Borhan, *J. Mater. Chem. C*, 2020, **8**, 16769–16773.
- M. S. Mudadu, A. N. Singh and R. P. Thummel, *J. Org. Chem.*, 2008, **73**, 6513–6520.
- G. Jiang, H. Liu, G. Ke, T. B. Ren, B. Xiong, X. B. Zhang and L. Yuan, *Angew. Chem., Int. Ed.*, 2024, **63**, e202315217.
- M. Stepień and L. Latos-Grazyński, *J. Am. Chem. Soc.*, 2002, **124**, 3838–3839.

